









Research Article

Improving SERS Sensing Efficiency and Catalytic Reduction Activity in Multifunctional Ternary Ag-TiO₂-GO Nanostructures: Roles of Electron Transfer Process on Performance Enhancement

Mai Quan Doan ¹, Nguyen Ha Anh ¹, Hoang Van Tuan ¹, Nguyen Cong Tu ²,
Nguyen Huu Lam ², Nguyen Tien Khi ^{1,3}, Vu Ngoc Phan ^{1,3}, Pham Duc Thang^{1,4}
and Anh-Tuan Le ^{1,4}

¹Phenikaa University Nano Institute (PHENA), Phenikaa University, Hanoi 12116, Vietnam

²School of Engineering Physics (SEP), Hanoi University of Science and Technology, Hanoi 10000, Vietnam

³Faculty of Biotechnology, Chemistry and Environmental Engineering, Phenikaa University, Hanoi 12116, Vietnam

⁴Faculty of Materials Science and Engineering, Phenikaa University, Hanoi 12116, Vietnam

Correspondence should be addressed to Mai Quan Doan; doan.maiquan@phenikaa-uni.edu.vn
and Anh-Tuan Le; tuan.leanh@phenikaa-uni.edu.vn

Received 10 August 2021; Revised 7 September 2021; Accepted 9 September 2021; Published 1 October 2021

Academic Editor: Ngo Nghia Pham

Copyright © 2021 Mai Quan Doan et al. This is an open access article distributed under the Creative Commons Attribution License, which permits unrestricted use, distribution, and reproduction in any medium, provided the original work is properly cited.

Multifunctional nanocomposites have received great attention for years; electron transfer (ET) is considered as an explanatory mechanism for enhancement of performance of these nanostructures. The existence of this ET process has been proved in many studies using either experimental or computational approaches. In this study, a ternary nanocomposite system of Ag/TiO₂/GO was prepared to evaluate the performance enhancement in two experimental models: a physical model (i.e., surface-enhanced Raman scattering (SERS) sensor) and a chemical one (i.e., catalytic reduction reaction). The metal/semiconductor heterojunction between Ag and TiO₂, as well as Ti-O-C bonds, has allowed plasmonic hot electrons to be transferred in the internal structure of the material. An investigation on the role of Ag content on the SERS sensing and catalytic reduction efficiency of Ag/TiO₂/GO was performed in both models. Interestingly, they all resulted in the same optimal Ag content of 50 wt%. It was then further discussed to provide a convincing evidence for the plasmon-induced electron transfer phenomena in the Ag/TiO₂/GO nanostructure. These findings also suggest a pathway to design and develop high-performance, cost-effective, facile-preparation, and eco-friendly multifunctional nanostructures for detecting and removing contaminants in environment.

1. Introduction

It is now widely accepted that electron-transfer (ET) mechanism in metal-semiconductor (MS) nanocomposites/nano-hybrids must be involved to explain the enhancement of their contaminant detection/degradation performance, in comparison to single metals or semiconductors [1–5]. ET naturally occurs in connection with the transduction of energy. In MS materials, ET process takes place in a dual-mode pathway. It means electrons can be transferred from metals to semiconductors or from semiconductors to metals,

which depends directly on the wavelengths of excitation sources [2–4, 6]. When a metal nanostructure contacts with a semiconductor, a specific space-charge region is created in MS interface, which leads to the band bending in the semiconductor and gives rise to a Schottky transition [2, 6]. Due to the light-matter interaction between ultraviolet (UV) light and the semiconductor, electrons are excited and then, they can be injected into the metal via the Schottky transition, causing the increase of the electron lifetime [6]. Meanwhile, localized surface plasmon resonance (LSPR) of the metal plays a central role in the generation of hot electrons when

interacting with a visible or infrared light, followed by injection of the hot electrons into the semiconductor [1, 3, 5]. As a result, a large number of active electrons were created, leading to the improvements in the efficiency of various applications such as sensing devices [4], photocatalysis [2], solar cells [3], photovoltaics [1], and photothermal therapies [5].

For several decades, many reports on ET process in MS structures, including both experimental and computational ones, have been published to clarify the importance of ET in the enhancement mechanisms of various technological applications [7–10]. For instance, Furube et al. utilized femtosecond transient absorption spectroscopy on Au/TiO₂ to observe plasmon-induced ET from Au nanodots to TiO₂ nanoparticles (NPs) [8]. Iida et al. proposed a directly transferred pathway of electrons from Ag nanoclusters to TiO₂ layers without passing through the conduction band of the Ag nanoclusters, using a computational approach [9]. Filipin et al. reported on another approach, in which they employed surface-enhanced Raman scattering (SERS) platform as an experimental model to investigate the enhanced Raman signals of R6G using TiO₂ nanotubes decorated with Ag NPs, resulting in 9×10^7 of Raman enhancement factor (EF) [7]. Yazid et al. investigated the enhanced catalytic reduction of 4-nitrophenol (4-NP) using AuNPs immobilized on the TiO₂ support; Au/TiO₂ exhibited superior catalytic activity in reduction of 4-NP, compared to AuNPs only [10]. Those reports have clarified the ET process in MS interfaces. However, each of those reports only focused on one kind of material for one specific application while ET process in MS materials may have led to the enhancement of the performance of various applications. Therefore, using different experimental models to investigate the enhancement of the performance efficiency of different applications with one material structure may answer the question if ET process in MS structures would exhibit the same effects on those distinct applications. Furthermore, it would provide more convincing evidence for the ET process in internal MS structures.

However, one of the main drawbacks of MS structures is their low adsorption capacity due to the poor adsorption capacity of their components (i.e., metals and semiconductors) [11]. Unfortunately, many popular applications including SERS sensors [12], photodegradation [13], and catalytic reaction [14] require an intimate interaction between the target molecules and the surface of the MS structures. Because of the poor adsorption capacity, only few target molecules can be adsorbed on MS surfaces to interact with active electrons, leading to the low performance of the applications using MS materials [12, 13]. Therefore, it is necessary to improve the adsorption capacity of MS materials to enhance their performance in those applications.

In the effort to find out an effective solution to improve the adsorption capacity of the MS structures, the introduction of graphene oxide (GO) to the nanocomposite structures has been regarded as a promising approach [15, 16]. GO is a two-dimensional carbon-based nanostructure which exhibits excellent adsorption capacity due to the presence of abundant oxygen functional groups such as hydroxyl, epoxy,

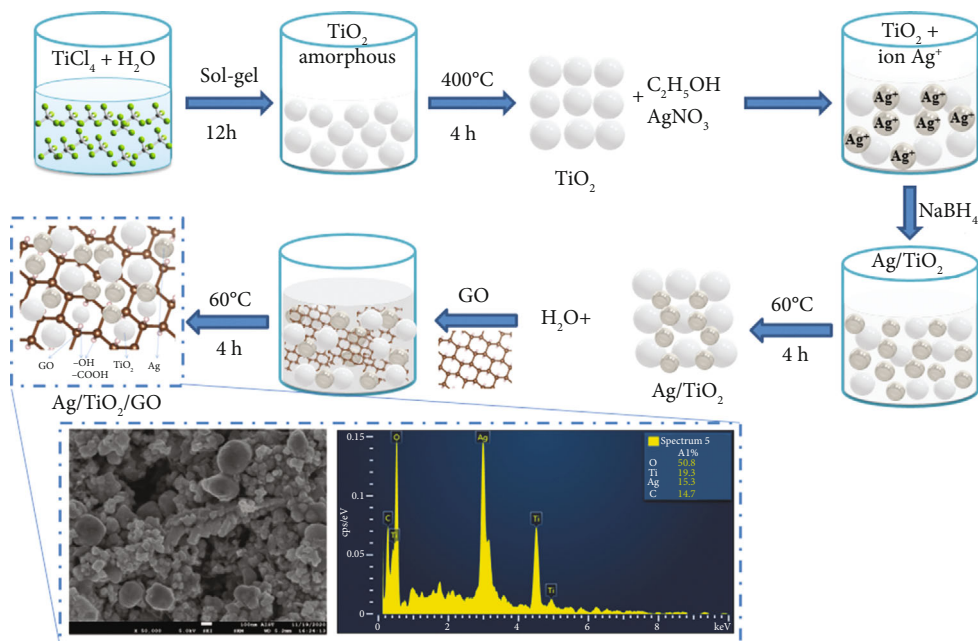
and carboxyl groups on its surface [16]. Wang et al. claimed that the photodegradation activity of TiO₂/GO composites was remarkably superior to that of TiO₂ due to the strong absorption capacity of GO [17]. In addition, GO can serve as an electron transporter. Gillespie et al. employed hybrid density functional theory calculations to propose that reduced-GO (rGO) in TiO₂/rGO had acted as a photoelectron trap (electron acceptor) via Ti-O-C bonds, leading to extended lifetimes of photoexcited charge carriers in TiO₂/rGO composites and improved photocatalytic efficiency [18]. Electrons should have continued to be transferred from TiO₂ to the GO sheets, leading to a stronger enhancement in the performance of TiO₂/rGO nanocomposites, in comparison to bare TiO₂ NPs. This study suggested an idea to fabricate other MS/GO nanocomposites, in which electrons can be transferred from metals to semiconductors and then GO sheets and improve the overall performance of their applications.

In this work, we prepared a set of Ag/TiO₂/GO nanocomposites (as MS/GO nanocomposites) to investigate their ET process. However, instead of focusing on specific measurements, such as femtosecond transient absorption spectroscopy [8], we stressed on the enhancement of the performance of the MS/GO structures and the repeat of this phenomenon in different experimental models. Thus, we aimed to discuss in detail about the correlation between the ET process and the performance of these empirical models. In more detail, we employed two experimental models including a physical model (i.e., SERS sensor) and a chemical model (i.e., catalytic reduction). Using a set of MS nanostructures that differed in Ag ratios, we further clarified the effects of Ag content in the composite structure on the performance of Ag/TiO₂/GO in each model. Moreover, the roles of TiO₂, GO in the performance enhancement were also discussed. The similar optimal Ag content in two models provided a convincing evidence for the ET process in multifunctional Ag/TiO₂/GO nanostructures.

2. Experimental Procedures

2.1. Materials. Silver nitrate (AgNO₃, ≥99.0 wt%), sodium borohydride (NaBH₄, 99 wt%), titanium tetrachloride (TiCl₄, ≥99.8 wt%), ammonium hydroxide (NH₄OH, 28.0–30.0% NH₃), ethanol (C₂H₅OH, 98 v/v%), methylene blue (MB, C₁₆H₁₈ClN₃S), and 4-nitrophenol (4-NP, C₆H₅NO₂) were purchased from Shanghai Chemical Reagent and used directly without further purification. Graphene oxide (GO) was prepared using a modified Hummers method. Double distilled water was used throughout the experiments.

2.2. Synthesis of Ag/TiO₂/GO Nanocomposites. Ag/TiO₂/GO nanocomposites (ATG Nces) were synthesized through a facile wet chemistry approach as described in Scheme 1. First, pure TiO₂ NPs were fabricated via a modified sol-gel method based on TiCl₄ precursors [19]. Gel solution was obtained by aging for 12 h at room temperature, followed by the annealing process at 400°C for 4 h, which induced the crystallization of TiO₂ NPs. The crystalline TiO₂ (0.2 g)



SCHEME 1: Schematic illustration of the synthesis steps for Ag/TiO₂/GO ternary nanocomposite.

was added into 50 ml of C₂H₅OH. Subsequently, to arrive at different Ag contents in the nanocomposites, 10 ml of AgNO₃ solution at different concentrations (62 mM, 91 mM, 185 mM, and 555 mM) was added to the solutions. The mixture was subjected to vigorous stirring at room temperature for 1 h, allowing the adsorption of Ag⁺ ions onto the TiO₂ NP's surface. A required 10 ml volume of NaBH₄ (62 mM, 91 mM, 185 mM, and 555 mM) was added to reduce ions Ag⁺ to Ag⁰ metals in each solution. After 2 hours of reduction, the as-synthesized Ag/TiO₂ NPs were purified by three washing cycles (1000 rpm) using deionized water and were dried at 60°C for 4 h. Then, GO nanosheets were synthesized using the modified Hummers' method reported by Paulchamy in 2015 [20]. A simple self-assembly approach was employed to decorate GO nanosheets with functional Ag/TiO₂ NPs. A homogeneous solution containing Ag/TiO₂ NPs was prepared by an ultrasonic homogenizer for 20 min. Then, the self-assembly of Ag/TiO₂ on the GO (3 ml, 2 mg/ml) surface occurred under constant stirring at 200 rpm for 2 h. Finally, we obtained a set of ATG Nces with varied ratios of Ag including 25, 33, 50, and 75 wt%, named as A1TG, A2TG, A3TG, and A4TG, respectively. GO content is fixed to be 6 wt% in every kind of ATG Nces investigated in this study.

2.3. Characterizations. The crystal phase and composition of Ag/TiO₂/GO were investigated by X-ray diffraction (Bruker D5005 X-ray diffractometer, Cu K_α, λ = 1.5406 Å) under a voltage of 40 kV and a current of 30 mA. The morphologies of Ag/TiO₂/GO were analyzed using scanning electron microscopy (SEM Hitachi S-4800) operating under an acceleration voltage of 5 kV and transmission electron microscopy (TEM JEOL JEM-1010) at an accelerating voltage of 80 kV. Chemical analyses of the nanocomposite were performed by Fourier-transform infrared spectroscopy (FTIR

HL ReactIR 45P), Raman spectroscopy (Horiba Macro-RAM™) with 785 nm laser excitation, and Energy Dispersive X-ray Spectroscopy (EDS). Optical analyses were carried out using a UV-Vis spectrophotometer (JENWAY 6850), and 10 mm path length quartz cuvettes were used for the measurements of absorption ranges.

2.4. Investigated Experimental Models: SERS Sensor, Catalytic Reduction. To investigate the enhanced electron transfer in ATG Nces, two experimental models with different electronic excitation/providing sources were undertaken. The first model was a SERS sensor based on the electronic excitation of a high-energy laser beam on Ag nanoparticles. To evaluate the SERS activity of ATG Nces, methylene blue (MB) was selected as a reporter molecule. Solutions at various concentrations of MB (10⁻⁴ to 10⁻⁹ M) were prepared in water. The substrates were fabricated through a few facile steps, in which square aluminum (Al) substrates were prepared with the dimension of 1 × 1 cm² and surface-active circular area with a diameter of 0.2 cm. ATG Nces with different contents of Ag was dispersed in water, then coated on the surface-active of Al substrate by a drop-casting method, and dried naturally at room temperature. MB reporter with various concentrations was dropped directly onto the ATG Nces-Al substrate, followed by the natural evaporation of water. SERS measurements were acquired via Raman spectroscopy under an excitation wavelength of 785 nm by means of a 100x objective lens with a 0.90 numerical aperture. The laser power was set to be 45 mW at 45° of contacting angle, with a diffraction-limited laser spot diameter of 1.1 μm (1.22 λ/NA, where λ is the wavelength of the laser, and NA is the numerical aperture of the microscope objective) and focal length of 115 nm. The expose time for each measurement was 10 seconds with 2 accumulations. A baseline calibration was conducted to obtain the final spectrum.

The second experimental model was based on the catalytic reduction property of ATG Nces with BH_4^- ions as an electron donor. The reduction of 4-nitrophenol (4-NP) to 4-aminophenol (4-AP) by NaBH_4 was selected as a model reaction for evaluating the catalytic reduction performance of our ATG Nces. First, 5 ml of 4-NP (2×10^{-4} M in water) was mixed with 5 ml NaBH_4 (0.01 M in water); the solution turned from light yellow to bright yellow rapidly. Subsequently, 0.8 mg of ATG Nces with different contents of Ag was added to the solution. Time-dependent absorption spectra were recorded by UV-Vis spectroscopy. The degradation rate catalytic reduction model was calculated by using the following equation:

$$\text{Percentage of degradation (\%)} = \frac{C_0 - C_t}{C_0} \times 100, \quad (1)$$

where C_0 and C_t represent, respectively, the initial 4-NP concentration and that at time t of degradation.

3. Results and Discussion

3.1. Characterizations of Ag/TiO₂/GO. Scheme 1 demonstrates the formation of ATG nanostructures. Firstly, the Ag/TiO₂ NPs were fabricated due to the reduction of Ag^+ ions adsorbed onto TiO₂ crystal matrix. Then, the as-synthesized Ag/TiO₂ NPs were self-assembled onto the surface of the GO sheets via electrostatic interactions. The morphology of ATG has been revealed in TEM and SEM images (Figure 1). Figure 1(a) shows the TEM image of ATG Nces with the presence of three types of materials with distinct shapes and sizes marked as Type 1, Type 2, and Type 3. Both Type 1 and Type 2 are spherical nanostructures but differed in size. The distribution histograms of SEM result shown in Figure 1(c) reveals the average diameters of Type 1 and Type 2 nanoparticles to be 50 nm and 100 nm with frequencies of 35% and 65%, respectively. Besides, Figure 1(b) shows the presence of Type 1 on the surface of Type 2. Thus, it can be assumed that Type 1 nanostructures represent Ag nanoparticles while Type 2 ones represent TiO₂ nanoparticles. In addition, Figure 1(c) and its magnified image (Figure 1(e)) also exhibit a sheet-like structure which reminds of the two-dimensional structure of GO-pristine (Figure 1(d)). The presence of Ag and TiO₂ nanoparticles on the surface of this sheet-like structure reveals the structure of Ag/TiO₂/GO, in which the Ag/TiO₂ nanostructures have been situated on the surface of GO sheets. The presence of GO in the nanocomposite can be also observed in the TEM image (Figure 1(a)) as large and plane nanostructures (Type 3).

The XRD pattern of ATG Nces is shown in Figure 2(a), in comparison with the reference patterns of TiO₂, Ag, and Ag/TiO₂. The position of the diffraction peaks at $2\theta = 38.010$, 44.09° , and 64.03° can be assigned to the (111), (200), and (220) planes of Ag NPs (ICDD file No. 01-087-0597), respectively. In addition, the XRD pattern also shows the diffractions of the crystal planes (101), (200), (211), (105), and (022) at $2\theta = 25.410$, 47.830 , 54.990 , 53.800 , and 62.660 , which correspond to anatase TiO₂ (ICDD file No.

01-086-1175). These results suggest successful formation of both Ag NPs and TiO₂ NPs in our as-synthesized composite nanomaterials. Furthermore, the diffraction peaks of ATG Nces are well-matched with those of Ag/TiO₂ (ICDD file No. 98-005-8369), which provides an evidence for the presence of Ag NPs in the TiO₂ crystal matrix. Besides, the Scherrer formula was employed to calculate the average crystal grain size of Ag NPs and TiO₂ NPs via their diffraction peaks [21]. The obtained results of 43 nm for Ag NPs and 125 nm for TiO₂ NPs have confirmed the assumptions about their sizes that we have provided from TEM and SEM analysis.

FTIR, Raman, and EDX spectra were recorded to analyze the chemical properties of ATG Nces. In the FTIR spectrum of ATG Nces (Figure 2(b)), the characteristic peaks of O–H stretching vibrations (3651 cm^{-1} , 3078 cm^{-1}) and C=O stretching vibrations (1715 cm^{-1}) are in agreement with the peaks observed in the FTIR of GO, including a broad band appeared at 3580 cm^{-1} and a sharp peak at 1640 cm^{-1} , respectively [22]. It can be ascribed to GO-containing ATG Nces. In addition, the characteristic peaks at 800 cm^{-1} and 467 cm^{-1} indicate to Ti–O–C bonding, which demonstrates the direct binding of TiO₂ onto the surface of GO sheets [23, 24]. Figure 2(d) shows Raman spectrum of ATG Nces, in comparison to those of GO and TiO₂. The Raman spectrum of the nanocomposite reveals two prominent peaks corresponding to D-band (1300 cm^{-1}) and G-band (1600 cm^{-1}) of GO, between which D-band is broad and higher in intensity compared to G-band. The ratio of intensities between D-band and G-band (I_D/I_G) of ATG Nces (1.6) is larger than that of GO-pristine (1.4). It has been reported that a broad D-band with higher relative intensity compared to that of G-band can be the result of high disorder in graphite [25]. The disorder of graphite in our materials may be due to the deposition of Ag/TiO₂ on the surface of GO sheets [25]. In addition, the two bands at 156 cm^{-1} and 635 cm^{-1} are also observed in the spectrum of TiO₂, which are assigned to the E_g modes of TiO₂ anatase phase. These Raman spectra have reconfirmed the presence of TiO₂ in the nanocomposite materials [26]. The chemical composition of the ATG Nces surface was studied by EDX spectroscopy. The EDX spectrum (Scheme 1) indicates the presence of Ag, Ti, O, and C and proves the high level of purity of ATG Nces. To analyze the optical properties of ATG Nces, UV-Vis absorption spectra were recorded (Figure 2(c)). The spectra of both TiO₂ and ATG Nces exhibit a significant absorption band in the UV region. However, the absorption spectrum of ATG Nces shows higher band intensity and a red-shift in the absorption edge. To clarify this difference in absorption edge, the optical bandgap of TiO₂ and ATG Nces were determined via Tauc plot (Figure 2(c), inset) using Kubelka-Munk function [27]. Tauc plot results indicate that the absorption edges in the spectra of TiO₂ and ATG Nces correspond to optical bandgaps of 3.15 eV and 2.83 eV, respectively. The difference in optical bandgap values between ATG Nces and TiO₂ can be explained by the interactions of TiO₂ and Ag (via attachment) and GO (via Ti–O–C bonding), which has been

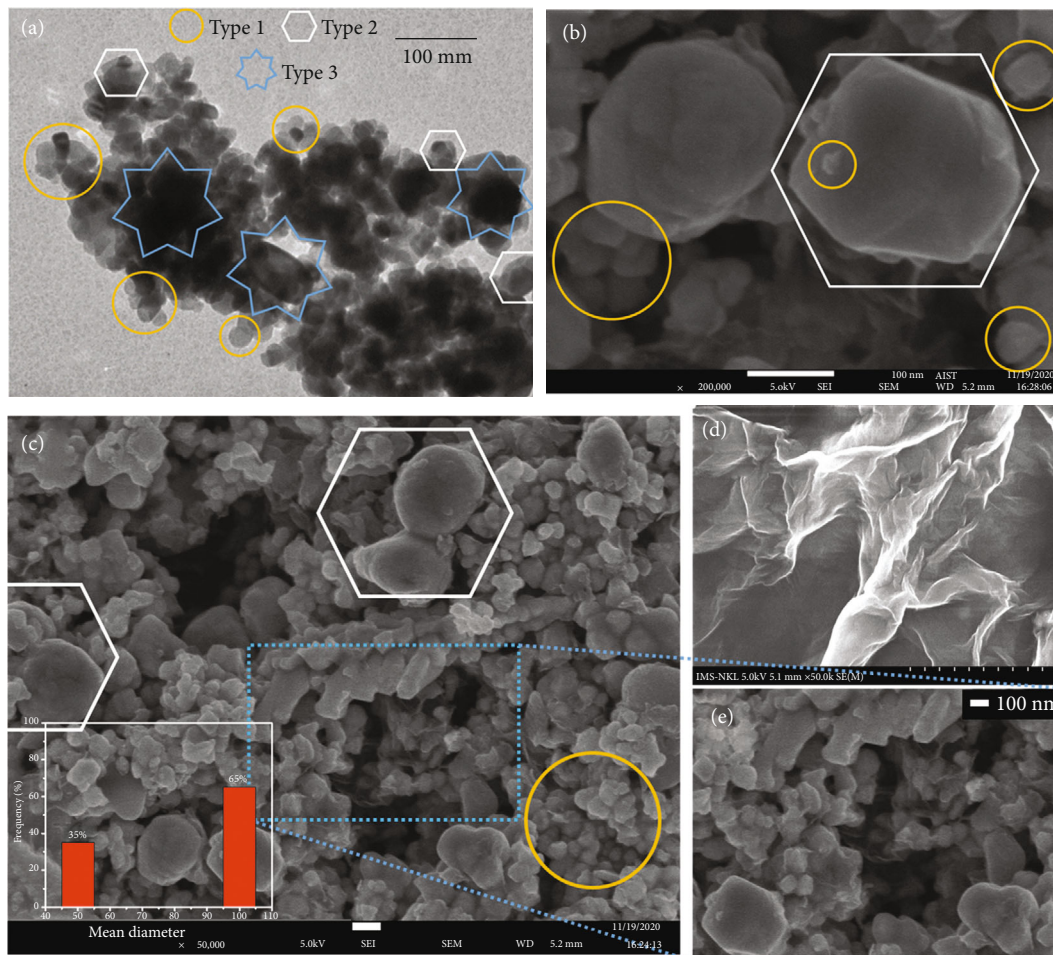


FIGURE 1: TEM image of (a) Ag/TiO₂/GO, (b, c, e) SEM images with different magnification and particle size distribution histograms of Ag/TiO₂/GO, and (d) GO-pristine.

confirmed by XRD and FTIR spectra, respectively. The formation of Ag/TiO₂ and Ti-O-C bonds has fulfilled all the requirements for the nanocomposite materials to be employed to study the electronic transfer process in their internal structures.

3.2. SERS Sensor Model. SERS sensor was the first model that we employed to investigate the enhanced electron transfer in ATG Nces, taking advantages of the unique plasmonic properties of Ag and enhanced Raman scattering caused by chemical enhancement of the nanocomposite materials [4, 12, 28]. As the plasmonic properties of Ag are the key to fabricate SERS sensors based on ATG Nces, a set of samples with distinct contents of Ag has been employed for SERS measurements as mentioned in Section 2, including A1TG, A2TG, A3TG, and A4TG. Figure 3(a) exhibits the SERS signals of MB in the presence of 4 kinds of nanomaterials as active substrates. On the substrate with 25 wt% of Ag (A1TG), the SERS spectrum reveals two characteristic peaks of GO (1300 cm⁻¹ and 1600 cm⁻¹) at high intensity. In contrast, the intensity of the characteristic peak of MB at 450 cm⁻¹ is much lower. In the increase of Ag contents, the SERS spectra of MB on A2TG and A3TG do not show such

significant peaks of GO but the characteristic peaks of MB at 450, 505, 1396, and 1620 cm⁻¹, which corresponds to vibrations of C-N-C skeletal deformation, C-S-C skeletal deformation, C-H in-plane ring deformation, and C-C stretching ring, respectively [29]. Unexpectedly, when the Ag content increases up to 75 wt%, the intensity of the characteristic peaks of MB suffered a great loss, compared to A3TG. It has to be stressed that the concentration of MB solution for every measurement was the same; thus, it is undeniable that the Ag content has a great effect on SERS activity of the nanocomposite material. In this case, the highest intensity of the MB characteristic bands allows A3TG to be the most SERS-effective substrate, compared to A1TG, A2TG, and A4TG.

Enhancement factor (EF) of ATG Nces with varied contents of Ag was calculated to further testify the SERS performance (Figure 3(a)). The SERS EF was observed in agreement with the previous report following the equation below [30]:

$$EF = \frac{I_{SERS}}{I_{Raman}} \times \frac{N_{bulk}}{N_{surface}}, \quad (2)$$

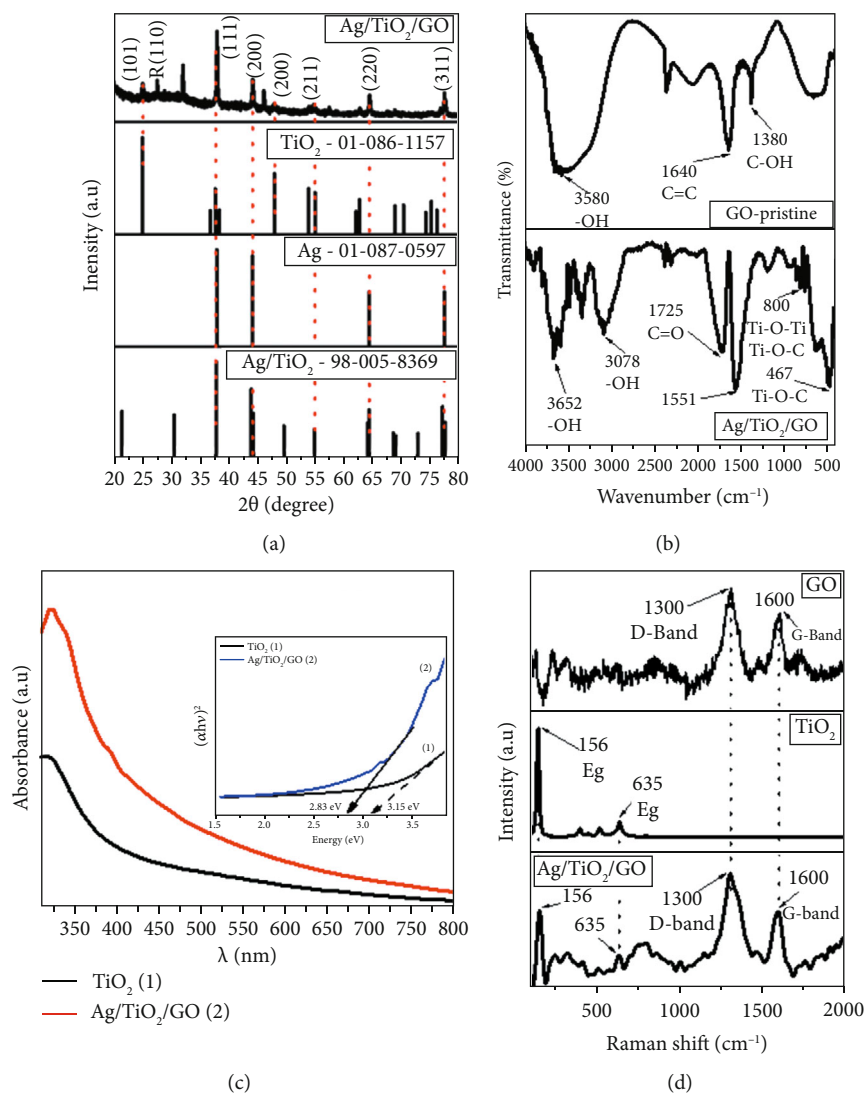


FIGURE 2: XRD pattern of Ag/TiO₂/GO (a), FTIR spectra of GO-pristine and Ag/TiO₂/GO (b), UV-Vis spectra and Tauc plot of TiO₂ and Ag/TiO₂/GO (c), Raman spectra of GO, TiO₂, and Ag/TiO₂/GO (d).

where I_{SERS} and I_{Raman} are Raman signal intensities of MB reporter with and without SERS from ATG Nces, respectively, and N_{bulk} is the average number of MB molecules in the scattering volume for the non-SERS measurement; N_{surface} is the number of the average number of MB molecules in the surface-active area for the SERS experiments (see Supporting information).

The EF values of A1TG, A2TG, A3TG, and A4TG were calculated to be 9.7×10^4 , 2.1×10^5 , 3.6×10^5 , and 1.3×10^5 , respectively. This calculation reconfirms that A3TG Nces is the highest SERS-effective substrate. In addition to the impressive enhancement factor of A3TG, the limit of detection for MB deposited on this SERS substrate was down to 0.93 nM with a linear range from 10^{-9} M to 10^{-4} M (Figure 3(b)). It is obvious that Ag content has a great effect on the performance of SERS sensor using ATG Nc substrates. In this case, the optimal Ag content is 50 wt%. Similar results have been reported in previous studies on other composites such as ternary Au@Cu₂O-Ag nanocomposite

and Ag-TiO₂ composite [31, 32]. In Section 3.1, we have pointed out that the formation of Ag/TiO₂ structures and Ti-O-C bonds, which might be convenient charge-separation pathways to increase the hot-electron age. Due to the local surface plasmon resonance (LSPRs) phenomenon, in which coherent electrons oscillate around the Ag NP surface formed hot electrons, it is reasonable that higher Raman intensity of MB was achieved when Ag content in ATG Nces increased (A1TG, A2TG, and A3TG). However, the unexpected decrease in the Raman signal of MB in the presence of A4TG might be explained by the surplus of Ag, which led to the decrease of TiO₂ and GO contents, as well as the formation of Ag/TiO₂ structures and Ti-O-C bonds. As a result, the electron transfer rate in the charge-separation pathway in the internal structure of ATG Nces might have been reduced. In addition, the EF value of A3TG is no more than 5 times higher than that of A1TG, A2TG, and A4TG. These small differences cannot be due to electromagnetic mechanism as it is usually related to large

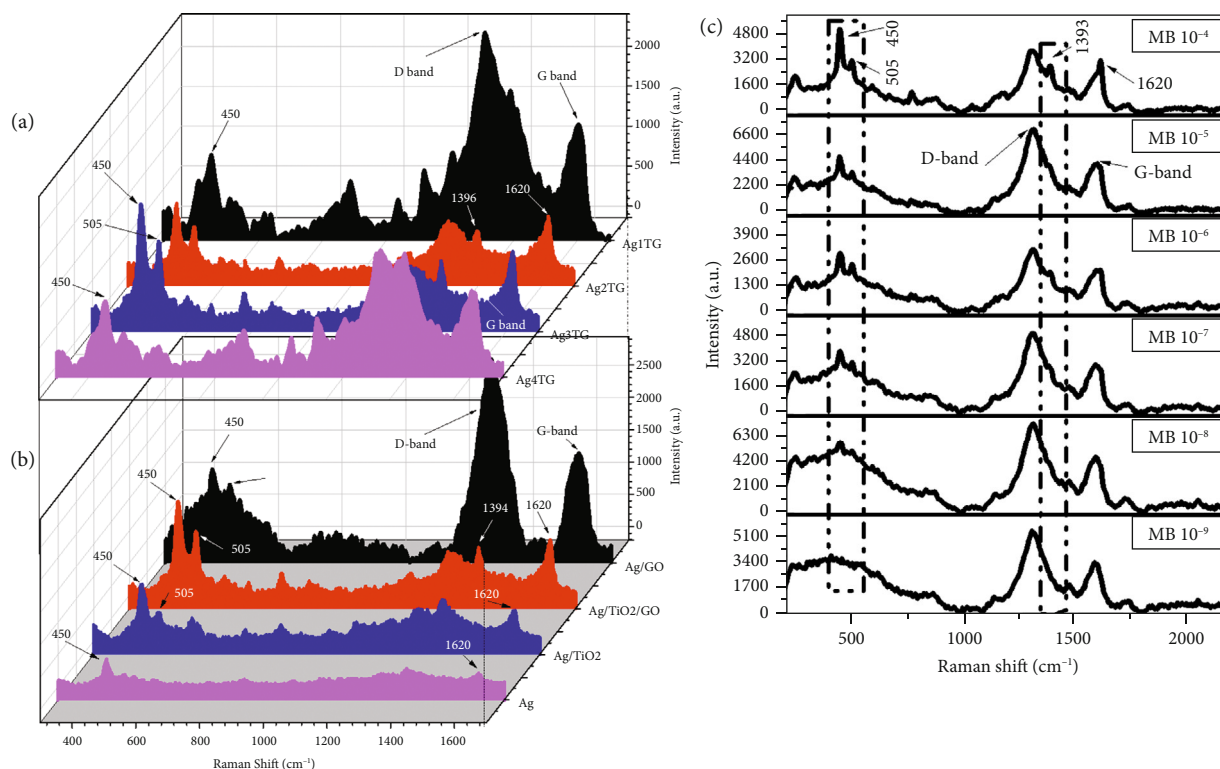


FIGURE 3: SERS spectra of MB (10^{-6} M) in the presence of ATG Nces with different Ag contents (A1TG, A2TG, A3TG, and A4TG) (a), and Ag-containing materials including Ag NPs, Ag/TiO₂, Ag/TiO₂/GO, and Ag/GO (b). SERS spectra of different concentrations of MB (10^{-4} – 10^{-9} M) in the presence of A3TG (c).

enhancement (10^6 – 10^{10} or even more) [30]. Instead, it can be explained by chemical mechanism, of which EFs are in the range of 10^1 – 10^3 [33]. It is worth mentioning that CM is directly related to electron transfer. Thus, in addition to the presence of Ag, the electron transfer through Ag/TiO₂ contacts and Ti-O-C bonds may be another factor causing the differences in the enhancement of Raman signal of MB on the ATG Nces containing varied Ag content.

The important role of TiO₂ and GO in the improvement of the SERS sensitivity of ATG Nces was confirmed by a comparison among the SERS spectra of MB (10^{-6} M) in the presence of only Ag NPs, Ag/TiO₂, Ag/GO, and Ag/TiO₂/GO (A3TG) (Figure 3(b)). Instead of 4 characteristic bands as mentioned previously, MB only exhibits 2 weak peaks at 450 cm⁻¹ and 1620 cm⁻¹ in the presence of only Ag NPs. The use of Ag/TiO₂ (50:50 wt%) obviously improves the sensitivity of the SERS sensing due to the presence of all characteristics. However, the intensity and the sharpness of the peaks are relatively lower than those using Ag/TiO₂/GO as SERS substrate. The utilization of Ag/GO also results in high intensity of SERS signal. However, D-band and G-band of GO overlap the peaks at 1393 cm⁻¹ and 1620 cm⁻¹ of MB while two other ones at 450 cm⁻¹ and 505 cm⁻¹ are not as clear as those in the use Ag/TiO₂/GO. This comparison has emphasized the role of TiO₂ and GO to enhance the SERS performance in the nanocomposite materials. Moreover, the materials achieved the highest efficiency in the presence of both TiO₂ and GO. It would confirm the hypothesis above about the impacts of the

electron transfer through Ag/TiO₂ contacts and Ti-O-C bonds of ATG Nces in their SERS performance improvement.

3.3. Catalytic Reduction Model. In addition to the physical model, we also generated a chemical one to answer the question of whether the electron transfer in the ATG Nces has any influences on other applications and how it affects their performance. A model of catalytic reduction was selected as its performance is directly related to electron transfer phenomena. The catalytic reduction model was studied through the reduction of 4-NP to 4-AP using NaBH₄ as an electronic providing source from BH₄⁻ to investigate the catalytic reduction properties of ATG Nces [34]. To clarify the role of TiO₂ and GO on the catalytic reduction performance of ATG Nces, we prepared two sets of samples. One set included Ag, Ag/TiO₂, Ag/GO, and Ag/TiO₂/GO. The other one consisted of ATG Nces containing varied Ag contents. The materials from each set were employed as catalysts for the reduction of 4-NP to 4-AP in the same experimental conditions as mentioned in Section 2.4. For each comparison, we used the same experimental conditions as the mass of catalyst material (0.8 mg), the concentration of 4-NP (2×10^{-4} M), NaBH₄ (0.01 M), and catalytic reduction reaction time (30 s). The absorption spectra of the reaction solutions in the presence of different catalysts were then recorded using UV-Vis spectroscopy. The peak at 400 nm in UV-Vis spectra, which is ascribed to 4-nitrophenolate ions, would be decreased gradually with time in the presence

of catalytic materials, signifying the degradation of 4-NP. Contemporaneously, the appearance of a new band at 300 nm represents the formation of 4-AP [34]. Figure 4 demonstrates the absorption spectra of the reaction samples using different catalytic materials in the two experimental sets.

Concerning the first set including Ag, Ag/TiO₂, Ag/GO, and Ag/TiO₂/GO, the 4-NP degradation efficiency of these four materials can be calculated based on the intensity of the absorption band at 400 nm (Figure 4(a)). Using Ag as the catalysts, the obtained absorption spectrum only exhibits a small decrease in the band at 400 nm, which represents the degradation efficiency of about 10% which is much lower than those of Ag/GO (~28%) and Ag/TiO₂ (~80%). Meanwhile, under the same reaction conditions, in the presence of Ag/TiO₂/GO, 4-NP was nearly completely degraded with the disappearance of the 400 nm band. The reduction of 4-NP to 4-AM is also confirmed by the increase in intensity of the 300 nm band. As expected, the absorption spectrum of reaction solution in the presence of Ag/TiO₂/GO shows the highest intensity at 300 nm, in comparison to the others. The differences in catalytic degradation efficiencies of the reaction using four distinct catalytic materials demonstrate the great effect of TiO₂ and GO on catalytic reduction performance of ATG Nces. In addition, Ag content also influences the performance of this application (Figure 4(b)). Thanks to the presence of Ag, TiO₂, and GO in the composite structures, it is not surprising that the 4-NP degradation efficiencies of A1TG, A2TG, A3TG, and A4TG are relatively high. However, the differences appear in the 300 nm band as the reaction solution using A3TG results in the highest intensity compared to the other one. Therefore, in the catalytic reduction model, 50% wt is still the optimal content of Ag in ATG Nces.

As negatively charged 4-nitrophenolate and BH₄⁻ preferably interact with the metallic catalyst and facilitate the hydrogenation process on the 4-nitrophenolate, it is obvious that Ag is the key component in ATG Nces, which has the highest effect on catalytic performance. However, the presence of TiO₂ in Ag/TiO₂ has also enhanced catalytic performance. Moreover, the addition of GO has continued improving this performance. When discussing about the characterization of ATG Nces and the SERS sensor model, we have demonstrated the formation of Ag/TiO₂ nanostructures and Ti-O-C bonds as well as their effects on SERS sensing efficiency. Once again, TiO₂ and GO have exhibited their importance in the performance of another application using the ATG Nces. Furthermore, the same optimal Ag content in ATG Nces in both SERS and catalytic reduction models suggests a similarity in the mechanism of performance enhancement in both models. As mentioned in the previous section, this mechanism is based on the separation pathway in the internal structure of ATG Nces through Ag/TiO₂ nanostructures and Ti-O-C bonds. It has been claimed in previous studies that when a metal oxide contacted with a metal intimately, a Schottky junction would be formed and Fermi level alignment would lead to charge redistribution, which was also known as the electron transfer process [2, 34]. Besides, other reports stated that an additional band edge and a

bandgap tuning were created due to the formation of Ti-O-C bonds and provided a conductive pathway for electron transfer from TiO₂ to GO [18, 35].

3.4. Relationship of SERS Sensor Model and Catalytic Reduction Model: Effects of Electron Transfer on Their Performance. The interesting similarity in optimal Ag content in both models has triggered us to further analyze the relationship between their performances and clarify the effect of electron transfer process on their performance. The comparisons of EFs in the SERS model and degradation efficiencies in the catalytic reduction model using ATG Nces with varied Ag contents are shown in Figures 5(a) and 5(b), respectively. A similar trend can be observed in the two graphs as EFs and degradation efficiencies both increase in the increase of Ag content and reach the highest peak at the content of 50 wt% (A3TG). Then, both of them decrease dramatically when the content of Ag rises to 75% (A4TG). Moreover, the similarity in impacts of TiO₂ and GO in the improvement of ATG Nces performance in both models is also worth mentioning. It may be an evidence for the ET pathway that will be further discussed in this section.

Concerning the SERS sensor model, according to quantum theory, when an incident laser light interacts with Ag NPs surface, Ag NPs serve as a light absorber, where hot electrons are generated due to by LSPR phenomenon [2]. Previous reports have stated that the specific interaction of the adsorbed MB molecule and the surface of Ag might lead to electron transfer from Ag to MB molecule, named metal to molecular transfer [12]. The superposition of energy levels should have been formed between Ag and adsorbed MB molecule [36]. The Fermi level of Ag was reported to be -4.26 eV [37], while the absolute energy of the lowest unoccupied molecular orbital (LUMO) of MB is -3.328 eV [38]. Thus, the plasmon-induced hot electrons can be transferred from Ag into the LUMO level of MB, then decay with the SERS signal of MB. However, the adsorbed surface area of Ag is relatively small and MB ions are positively charged, so the absorption of MB on the Ag surface can be prevented. Therefore, that ET process should not have been completely responsible for the obtained SERS signal enhancement of our materials. This hypothesis has been confirmed by a significant loss of SERS signal when using the ATG Nces with surplus Ag content. Another ET pathway in the internal structure of ATG Nces, the metal-semiconductor transition, might have taken the lead in this case. Wu et al. proposed the ET pathway in a study about a system of CdSe-Au hetero-nanostructures and named this hot-electron transfer pathway a plasmon-induced interfacial charge-transfer transition (PICTT) to discriminate against the common plasmon-induced hot-electron transfer (PHET) or direct metal-to-semiconductor interfacial charge-transfer transition (DICTT) [39]. In PICTT, the metal serves as a light absorber, but strong interdomain coupling and mixing of the metal and semiconductor levels lead to a new plasmon decay pathway. Besides, PICTT also exhibits the quantum efficiency to be higher than 24%. In addition, Iida and Noda reported on the photoinduced silver-TiO₂ electronic interaction that allowed the excited electrons to be directly

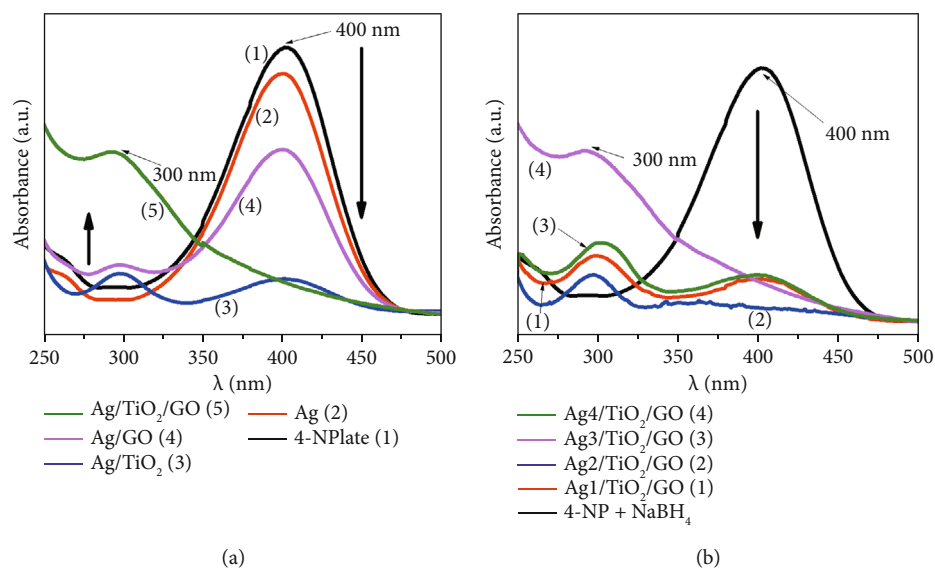


FIGURE 4: UV-Vis spectra of the catalytic reduction of 4-nitrophenolate (400 nm) to 4-aminophenol (300 nm) in the water and comparison of catalytic efficiency of Ag, Ag/TiO₂, Ag/GO, and Ag/TiO₂/GO (a); comparison of catalytic efficiency of varied contents of Ag in ATG Nces (b).

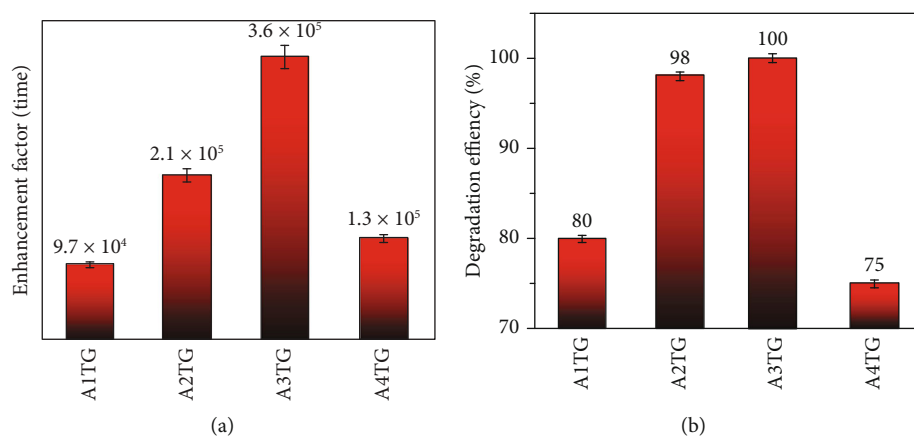


FIGURE 5: Comparison of enhancement factor (at 10⁻⁶ M) (a) and degradation efficiency (b) of Ag/TiO₂/GO with different Ag contents.

transferred from the silver nanocluster to the TiO₂ layer without passing through the conduction band of the silver nanocluster. Nevertheless, it might potentially occur due to the formation of Ag-O bonds between the silver-TiO₂ layers [9] while in our nanocomposites, Ag and TiO₂ only form a weak interaction due to natural deposition. Thus, the PHET pathway might be the more suitable mechanism that has occurred in our materials. In PHET, the metal decays into a hot electron-hole pair through Landau damping, followed by injection of the hot electrons into the conduction band (CB) of the semiconductor [40]. Here, electrons might have been transferred through Ag/TiO₂ interaction (Schottky junction). Moreover, TiO₂ is an excellent electron acceptor via d-orbital [41]. In addition, plasmon-induced hot electrons can inject into CB of TiO₂ with conduction band minimum energy of -4.0 eV [42]. Therefore, the transferred electrons have more opportunities to interact with MB molecule. Nevertheless, electron transfer process in CB of TiO₂

competes with electron relaxation through rapid electron-electron scattering. Then again, Ti-O-C might have been allowed electrons to be transferred from TiO₂ to GO sheets, whose Fermi level is -5.02 eV [25]. Since GO is an excellent adsorber [16], the GO sheets might have increased the direct interaction between hot electrons to MB molecular. As a result, many active electrons have interacted with MB reporters via the charge-separation pathways in ATG Nces; thus, the Raman signal of MB has been enhanced by the chemical mechanism.

Concerning the catalytic reduction model, the potential charge-separation pathway in ATG Nces should have been an important factor to lead to the enhancement of 4-NP degradation efficiency. Due to the adsorption of negatively charged BH₄⁻ on the surface of Ag NPs, BH₄⁻ ions acted as electron donors that provided active electrons to Ag. In the same electron transfer pathway as in the SERS sensor model, electrons would have escaped from Ag and

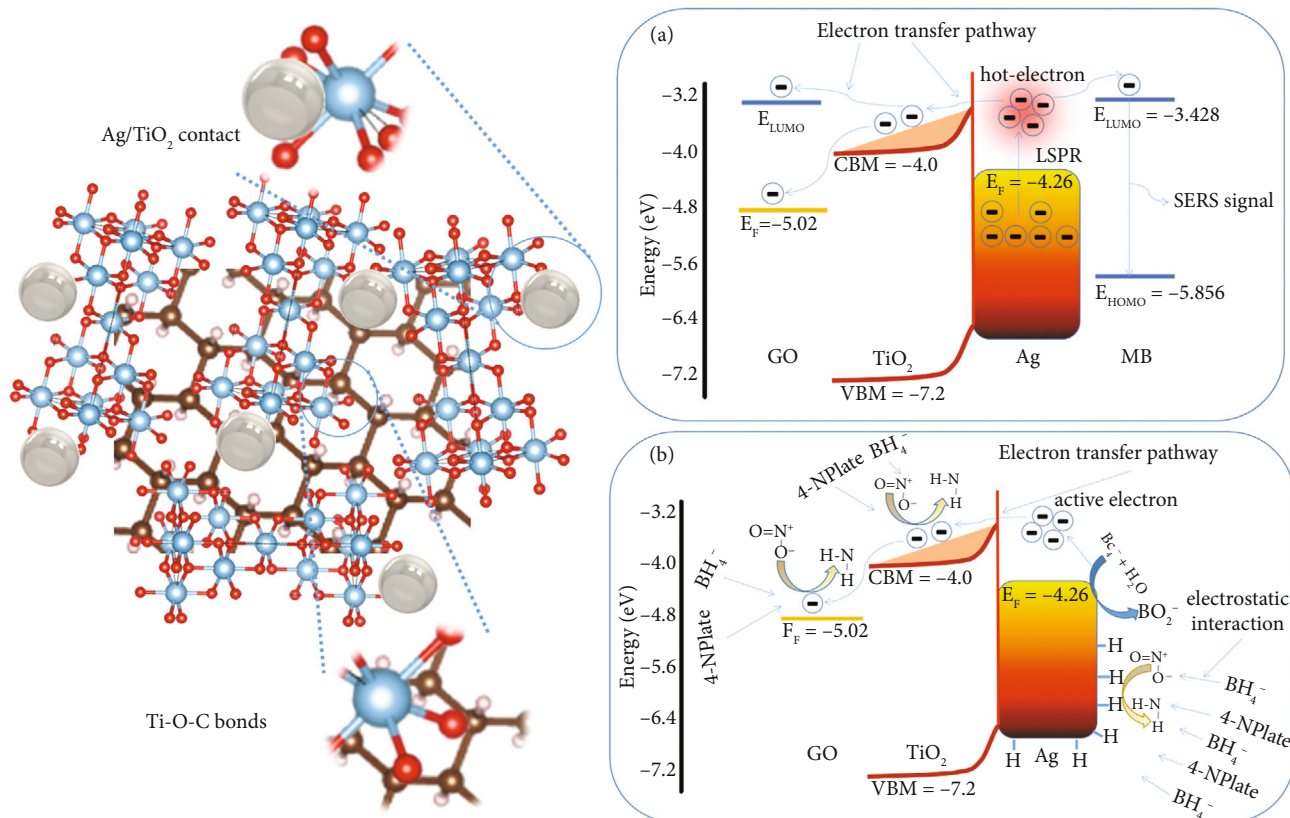


FIGURE 6: Potential electron transfer process in ATG Nces for both SERS sensor model (a) and catalytic reduction model (b) through Ag/TiO₂ contact and Ti-O-C bonds.

TABLE 1: Several reported AgNP-based SERS sensors to determine MB and their sensing performance (LOD, EF; nanoparticles (NPs); graphene foam (GF); nanotube array (NTA); 4-mercaptobenzoic acid (4-MBA).

Materials	Analyte	Substrate	LOD	EF	References
AgNPs/GF	MB	Si	10 ⁻⁹ (M)	5 × 10 ⁴	[43]
Au@Cu ₂ O-Ag	4-MBA	—	10 ⁻⁹ (M)	7.19 × 10 ⁵	[31]
GO/Ag/TiO ₂ NTA	MB	—	10 ⁻⁹ (M)	2.1 × 10 ⁷	[44]
Ag/TiO ₂ /GO	MB	Al	3.32 × 10 ⁻¹⁰ (M)	7.3 × 10 ⁴	This work

TABLE 2: Comparison catalytic performance of several reported AgNP-based nanomaterials to remove 4-NP (concentration, reaction time, and removal performance); poly(acrylic acid) (PPA); reduced-GO (rGO); cellulose nanocrystals (CNC).

Catalyst	4-NP (M)	NaBH ₄ (M)	Reaction time	Removal efficiency (%)	References
Ag@PPA	10 ⁻⁴	0.1	300 s	100	[45]
Ag-rGO	5 × 10 ⁻⁵	0.1	360 s	98	[46]
CuFe ₂ O ₄ /CNC@Ag	5 × 10 ⁻³	0.1	360 s	100	[34]
Ag/TiO ₂ /GO	2 × 10 ⁻⁴	0.01	20 s	100	This work

transferred into TiO₂ and GO sheets. Zhang et al. suggested that electron transfer between Ag and CuFe₂O₄ led to the surplus electrons on CuFe₂O₄, which facilitated the capture of electrons by 4-NP molecules [34]. Herein, the transferred electrons in the GO sheets and TiO₂ might have provided a

large active-surface area to capture more BH₄⁻ and 4-nitrophenolate ions, thus, increased the rate of the catalytic reduction reaction.

In summary, the Ag content has a great effect on the electron transfer process in the internal nanostructure of

ATG Nces; therefore, it also influences the performance of SERS and catalytic reduction of ATG Nces. The same optimal Ag content, as well as the similar trend of performance changing observed in the presence of ATG Nces containing varied Ag content in those two models, has demonstrated the important role of electron transfer in the enhancement of their performance. Through the SERS sensor model and the catalytic reduction model, we propose a potential electron transfer pathway in ATG Nces via Ag/TiO₂ interaction and Ti-O-C bonds, which is exhibited in Figure 6.

Thanks to the ET process, the performance of ATG Nces materials in different applications has been enhanced. With a low LOD of 0.93 nM, our ATG Nces-based SERS sensor for MB detection is capable to determine MB at extremely low levels. Table 1 presents the comparison in SERS sensibility among ATG Nces and several reported materials, in which ATG Nces-based sensor results in the lowest LOD. It suggests the development of high-performance SERS sensors using this nanocomposite material as the substrate for detection of other contaminants. Moreover, ATG Nces also exhibit excellent 4-NP removal efficiency via catalytic reduction reaction with 100% of 4-NP degraded after 20 s, which is competitive in comparison to several reported catalytic materials (Table 2). Similarly, the performance of other applications related to the electron transfer pathway, such as photocatalysis, electrocatalysts, and solar cells, might be also enhanced with the utilization of ATG Nces. Thus, with a few facile steps of preparation as mentioned in Section 2, we can fabricate a multifunctional material that consists of nontoxic components (i.e., Ag, TiO₂, and GO). Furthermore, the synthesis can be scaled up to increase the mass production and reduce the cost of the fabrication. It suggests a direction to fabricate multifunctional, high-performance, cost-effective, facile-preparation, and nontoxic materials for detecting and removing contaminants.

4. Conclusions

In this work, Ag/TiO₂/GO Nces were successfully synthesized. The SEM, TEM, XRD, FTIR, Raman, UV-Vis, and EDX results confirmed the formation of Ag/TiO₂ structure and the deposition of Ag/TiO₂ on GO nanosheets via Ti-O-C bonds. We investigated the electron transfer process in Ag/TiO₂/GO Nces using two experimental models including SERS sensor and catalytic reduction, in which the Ag/TiO₂/GO Nces acted as SERS substrates and catalysts. The optimal Ag content of 50 wt% was appropriate in both models. From these results, we proposed a charge-separation pathway in the internal structure of ATG Nces that is suitable for both models. This study provides a clear explanation for the electron transfer process in composite nanostructures which leads to the enhancement of application efficiencies.

Data Availability

Data are available on request.

Conflicts of Interest

The authors declare that they have no known competing financial interests or personal relationships that could have appeared to influence the work reported in this paper.

Authors' Contributions

M. Q. Doan and N. H. Anh contributed equally to this work.

Acknowledgments

This research was supported by the Vietnam National Foundation for Science and Technology Development (NAFOSTED) through a fundamental research project (103.02-2018.50). The authors would like to acknowledge the supports with Raman, UV-Vis measurements from NEB Lab at the Phenikaa University.

Supplementary Materials

Figure S1: regression equation expressing the linear relationship between concentration of 4-nitrophenolate and absorption intensity of the reaction solution. Calculation of limit of detection (LOD-SERS sensor model). Figure S2: plot of Log of SERS intensity against Log of analyte concentration at 450 cm⁻¹, 505 cm⁻¹, 1393 cm⁻¹, and 1620 cm⁻¹. Calculation of enhancement factor (EF-SERS sensor model). (*Supplementary Materials*)

References

- [1] H. Atwater and A. Polman, "Plasmonics for improved photovoltaic devices," *Nature Mater.*, vol. 9, pp. 205–213, 2010.
- [2] C. Clavero, "Plasmon-induced hot-electron generation at nanoparticle/metal-oxide interfaces for photovoltaic and photocatalytic devices," *Nature Photonics*, vol. 8, no. 2, pp. 95–103, 2014.
- [3] J. Li, S. K. Cushing, F. Meng, T. R. Senty, A. D. Bristow, and N. Wu, "Plasmon-induced resonance energy transfer for solar energy conversion," *Nature Photonics*, vol. 9, no. 9, pp. 601–607, 2015.
- [4] H. Zhang, J. Wei, X.-G. Zhang et al., "Plasmon-induced interfacial hot-electron transfer directly probed by Raman spectroscopy," *Chem*, vol. 6, no. 3, pp. 689–702, 2020.
- [5] T. Zheng, T. Zhou, X. Feng, J. Shen, M. Zhang, and Y. Sun, "Enhanced plasmon-induced resonance energy transfer (PIRET)-mediated photothermal and photodynamic therapy guided by photoacoustic and magnetic resonance imaging," *ACS Applied Materials & Interfaces*, vol. 11, no. 35, pp. 31615–31626, 2019.
- [6] A. Bumajdad and M. J. P. C. C. P. Madkour, "Understanding the superior photocatalytic activity of noble metals modified titania under UV and visible light irradiation," *Physical Chemistry Chemical Physics*, vol. 16, no. 16, p. 7146, 2014.
- [7] N. Filippin, J. Castillo-Seoane, M. C. López-Santos et al., "Plasma-enabled amorphous TiO₂ Nanotubes as hydrophobic support for molecular sensing by SERS," *ACS Applied Materials & Interfaces*, vol. 12, no. 45, pp. 50721–50733, 2020.
- [8] A. Furube, L. du, K. Hara, R. Katoh, and M. Tachiya, "Ultrafast plasmon-induced electron transfer from gold nanodots into

- TiO₂Nanoparticles,” *Journal of the American Chemical Society*, vol. 129, no. 48, pp. 14852–14853, 2007.
- [9] K. Iida and M. Noda, “Electron transfer governed by light-matter interaction at metal- semiconductor interface,” *npj Computational Materials*, vol. 6, no. 1, 2020.
- [10] H. Yazid, N. A. A. Rahman, and A. M. M. Jani, “Catalytic reduction of p-nitrophenol on Au/TiO₂ powder and Au/TiO₂ membrane,” *AIP Conference Proceedings*, vol. 2332, p. 070004, 2021.
- [11] M. Manyangadze, N. Chikuruwo, T. B. Narsaiah, C. S. Chakra, M. Radhakumari, and G. Danha, “Enhancing adsorption capacity of nano-adsorbents via surface modification: a review,” *South African Journal of Chemical Engineering*, vol. 31, pp. 25–32, 2020.
- [12] A. M. Michaels, M. Nirmal, and L. E. Brus, “Surface enhanced Raman spectroscopy of individual rhodamine 6G molecules on large Ag nanocrystals,” *Journal of the American Chemical Society*, vol. 121, no. 43, pp. 9932–9939, 1999.
- [13] F. Azeez, E. al-Hetlani, M. Arafa et al., “The effect of surface charge on photocatalytic degradation of methylene blue dye using chargeable titania nanoparticles,” *Scientific Reports*, vol. 8, no. 1, 2018.
- [14] J. Sun, J. Zhang, H. Fu et al., “Enhanced catalytic hydrogenation reduction of bromate on Pd catalyst supported on CeO₂ modified SBA-15 prepared by strong electrostatic adsorption,” *Applied Catalysis B: Environmental*, vol. 229, pp. 32–40, 2018.
- [15] H. Lai, F. Xu, Y. Zhang, and L. Wang, “Recent progress on graphene-based substrates for surface-enhanced Raman scattering applications,” *Journal of Materials Chemistry B*, vol. 6, no. 24, pp. 4008–4028, 2018.
- [16] S. Thangavel and G. J. P. Venugopal, “Understanding the adsorption property of graphene-oxide with different degrees of oxidation levels,” *Powder Technology*, vol. 257, pp. 141–148, 2014.
- [17] R. Wang, K. Shi, D. Huang, J. Zhang, and S. An, “Synthesis and degradation kinetics of TiO₂/GO composites with highly efficient activity for adsorption and photocatalytic degradation of MB,” vol. 9, no. 1, 2019.
- [18] P. N. Gillespie and N. Martsinovich, “Origin of charge trapping in TiO₂/reduced graphene oxide photocatalytic composites: insights from theory,” *ACS Applied Materials & Interface*, vol. 11, no. 35, pp. 31909–31922, 2019.
- [19] M. E. Simonsen and E. G. Sogaard, “Sol-gel reactions of titanium alkoxides and water: influence of pH and alkoxy group on cluster formation and properties of the resulting products,” *Journal of Sol-Gel Science and Technology*, vol. 53, no. 3, pp. 485–497, 2010.
- [20] B. Paulchamy, G. Arthi, and B. D. Lignesh, “A simple approach to stepwise synthesis of graphene oxide nanomaterial,” *Journal of Nanomedicine & Nanotechnology*, vol. 6, no. 1, 2015.
- [21] U. Holzwarth and N. Gibson, “The Scherrer equation versus the ‘Debye-Scherrer equation,’” *Nature Nanotechnology*, vol. 6, no. 9, pp. 534–534, 2011.
- [22] D. Khalili, “Graphene oxide: a promising carbocatalyst for the regioselective thiocyanation of aromatic amines, phenols, anisols and enolizable ketones by hydrogen peroxide/KSCN in water,” *New Journal of Chemistry*, vol. 40, no. 3, pp. 2547–2553, 2016.
- [23] L. C. Sim, K. H. Leong, S. Ibrahim, and P. Saravanan, “Graphene oxide and Ag engulfed TiO₂nanotube arrays for enhanced electron mobility and visible-light-driven photocatalytic performance,” *Journal of Materials Chemistry A*, vol. 2, no. 15, pp. 5315–5322, 2014.
- [24] H. Zhang, X. Wang, N. Li et al., “Synthesis and characterization of TiO₂/graphene oxide nanocomposites for photoreduction of heavy metal ions in reverse osmosis concentrate,” *RSC Advances*, vol. 8, no. 60, pp. 34241–34251, 2018.
- [25] W. Su, N. Kumar, A. Krayev, and M. Chaigneau, “In situ topographical chemical and electrical imaging of carboxyl graphene oxide at the nanoscale,” *Nature Communications*, vol. 9, pp. 1–7, 2018.
- [26] M. Ceballos-Chuc, C. Ramos-Castillo, J. Alvarado-Gil, G. Oskam, and G. Rodríguez-Gattorno, “Influence of brookite impurities on the Raman spectrum of TiO₂Anatase nanocrystals,” *The Journal of Physical Chemistry C*, vol. 122, no. 34, pp. 19921–19930, 2018.
- [27] P. Makuła, M. Pacia, and W. Macyk, *How to Correctly Determine the Band Gap Energy of Modified Semiconductor Photocatalysts based on UV-Vis Spectra*, ACS Publications, 2018.
- [28] Y. Liu, H. Ma, X. X. Han, and B. Zhao, “Metal-semiconductor heterostructures for surface-enhanced Raman scattering: synergistic contribution of plasmons and charge transfer,” *Materials Horizons*, vol. 8, pp. 370–382, 2021.
- [29] X. Guo, Z. Guo, Y. Jin, Z. Liu, W. Zhang, and D. Huang, “Silver-gold core-shell nanoparticles containing methylene blue as SERS labels for probing and imaging of live cells,” *Microchimica Acta*, vol. 178, no. 1-2, pp. 229–236, 2012.
- [30] E. C. le Ru, E. Blackie, M. Meyer, and P. G. Etchegoin, “Surface enhanced Raman scattering enhancement factors: a comprehensive study,” *The Journal of Physical Chemistry C*, vol. 111, no. 37, pp. 13794–13803, 2007.
- [31] T. Wu, H. Zheng, Y. Kou et al., “Self-sustainable and recyclable ternary Au@Cu₂O-Ag nanocomposites: application in ultrasensitive SERS detection and highly efficient photocatalysis of organic dyes under visible light,” *Microsystems & Nanoengineering*, vol. 7, no. 1, p. 23, 2021.
- [32] Y. Zhang, F. Fu, Y. Li, D. Zhang, and Y. Chen, “One-step synthesis of Ag@TiO₂ nanoparticles for enhanced photocatalytic performance,” *Nanomaterials*, vol. 8, no. 12, p. 1032, 2018.
- [33] V. Shvalya, G. Filipič, J. Zavašnik, I. Abdulhalim, and U. Cvelbar, “Surface-enhanced Raman spectroscopy for chemical and biological sensing using nanoplasmonics: the relevance of interparticle spacing and surface morphology,” *Applied Physics Reviews*, vol. 7, no. 3, article 031307, 2020.
- [34] S. Zhang, Y. Xu, D. Zhao, W. Chen, H. Li, and C. Hou, “Preparation of magnetic CuFe₂O₄@Ag@ZIF-8 nanocomposites with highly catalytic activity based on cellulose nanocrystals,” *Molecules*, vol. 25, no. 1, p. 124, 2020.
- [35] Q. Zhang, N. Bao, X. Wang et al., “Advanced fabrication of chemically bonded graphene/TiO₂ continuous fibers with enhanced broadband photocatalytic properties and involved mechanisms exploration,” *Scientific Reports*, vol. 6, no. 1, article 38066, 2016.
- [36] L. Jensen, C. M. Aikens, and G. C. Schatz, “Electronic structure methods for studying surface-enhanced Raman scattering,” *Chemical Society Reviews*, vol. 37, no. 5, pp. 1061–1073, 2008.
- [37] H. B. Michaelson, “The work function of the elements and its periodicity,” *Journal of Applied Physics*, vol. 48, no. 11, pp. 4729–4733, 1977.
- [38] M. Alshabib, M. A. Oluwadamilare, A. Tanimu, I. Abdulazeez, K. Alhooshani, and S. A. Ganiyu, “Experimental and DFT investigation of ceria-nanocomposite decorated AC derived

- from groundnut shell for efficient removal of methylene-blue from wastewater effluent,” *Applied Surface Science*, vol. 536, p. 147749, 2021.
- [39] K. Wu, J. Chen, J. R. McBride, and T. Lian, “Efficient hot-electron transfer by a plasmon-induced interfacial charge-transfer transition,” *Science*, vol. 349, no. 6248, pp. 632–635, 2015.
- [40] A. O. Govorov, H. Zhang, and Y. K. Gun’ko, “Theory of photo-injection of hot plasmonic carriers from metal nanostructures into semiconductors and surface molecules,” *The Journal of Physical Chemistry C*, vol. 117, no. 32, pp. 16616–16631, 2013.
- [41] R. Katoh, A. Furube, T. Yoshihara et al., “Efficiencies of electron injection from excited N3 dye into nanocrystalline semiconductor (ZrO₂, TiO₂, ZnO, Nb₂O₅, SnO₂, In₂O₃) films,” *The Journal of Physical Chemistry B*, vol. 108, no. 15, pp. 4818–4822, 2004.
- [42] M. Parashar, V. K. Shukla, and R. Singh, “Metal oxides nanoparticles via sol–gel method: a review on synthesis, characterization and applications,” *Journal of Materials Science: Materials in Electronics*, vol. 31, pp. 3729–3749, 2020.
- [43] C. Srichan, M. Ekpanyapong, M. Horprathum et al., “Highly-sensitive surface-enhanced Raman spectroscopy (SERS)-based chemical sensor using 3D graphene foam decorated with silver nanoparticles as SERS substrate,” *Scientific Reports*, vol. 6, no. 1, article 23733, 2016.
- [44] Y. Xie and Y. Meng, “SERS performance of graphene oxide decorated silver nanoparticle/titania nanotube array,” *RSC Advances*, vol. 4, no. 79, pp. 41734–41743, 2014.
- [45] C. Kästner and A. F. Thünemann, “Catalytic reduction of 4-nitrophenol using silver nanoparticles with adjustable activity,” *Langmuir*, vol. 32, no. 29, pp. 7383–7391, 2016.
- [46] Y. Y. Liu, Y. H. Zhao, Y. Zhou et al., “High-efficient catalytic reduction of 4-nitrophenol based on reusable Ag nanoparticles/graphene-loading loofah sponge hybrid,” *Nanotechnology*, vol. 29, no. 31, p. 315702, 2018.